Quantitative Phosphoproteomics Analysis Uncovers PAK2- and CDK1-Mediated Malignant Signaling Pathways in Clear Cell Renal Cell Carcinoma

Authors

Aydanur Senturk, Ayse T. Sahin, Ayse Armutlu, Murat Can Kiremit, Omer Acar, Selcuk Erdem, Sidar Bagbudar, Tarik Esen, and Nurhan Ozlu

Correspondence

nozlu@ku.edu.tr

Graphical Abstract

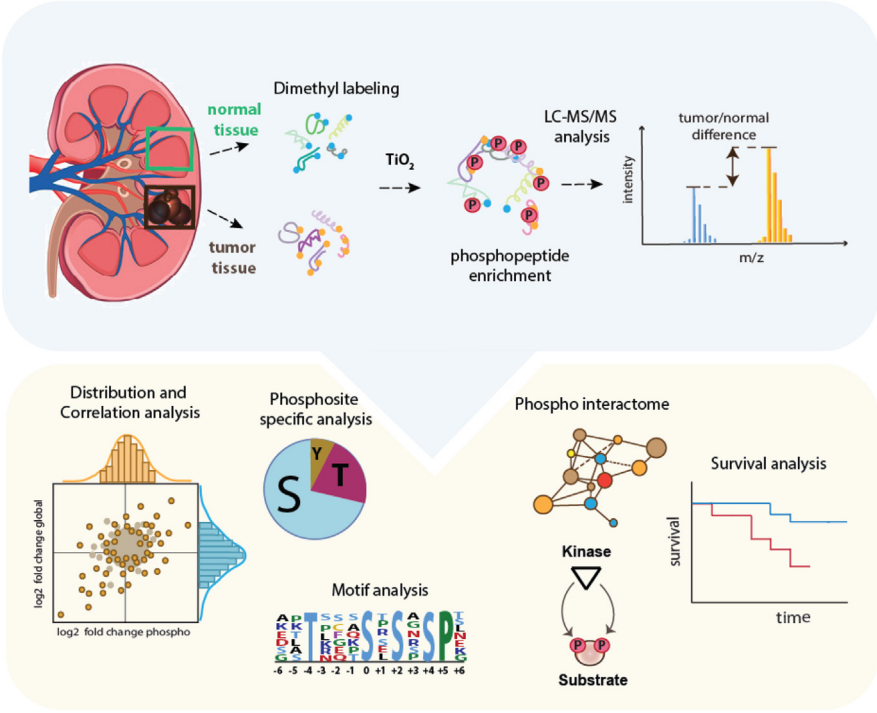

In Brief

Senturk *et al.* (2022) identified >16,000 phosphopeptides in clear cell Renal Cell Carcinoma tumors, of which 600 were determined to be differentially regulated between tumor and normal adjacent tissues. Furthermore, several oncogenic pathways were determined to be enriched in the tumors such as RAC1 activation, MAPK and VEGF signaling, EGFR signaling, and cytokine signaling. Moreover, the kinase PAK2 was identified as one of the key drivers of tumor migration and invasion, having prognostic impact on the survival of ccRCC patients.

Highlights

- More than 16,000 phosphopeptides identified in clear cell Renal Cell Carcinoma tumors.
- Mesenchymal profile implies increased migratory behavior of ccRCC tumors.
- PAK2 and CDK1 are undescribed key kinases in ccRCC tumorigenesis.
- High expression of PAK2 leads to significantly worse survival of ccRCC patients.

2022, Mol Cell Proteomics *21*(*11*), 100417

https://doi.org/10.1016/j.mcpro.2022.100417

Quantitative Phosphoproteomics Analysis Uncovers PAK2- and CDK1-Mediated Malignant Signaling Pathways in Clear Cell Renal Cell Carcinoma

Aydanur Senturk[1], Ayse T. Sahin[1], Ayse Armutlu[2], Murat Can Kiremit[3], Omer Acar[3], Selcuk Erdem[4], Sidar Bagbudar[5], Tarik Esen[3], and Nurhan Ozlu[1,6,*]

Clear cell Renal Cell Carcinoma (ccRCC) is among the 10 most common cancers in both men and women and causes more than 140,000 deaths worldwide every year. In order to elucidate the underlying molecular mechanisms orchestrated by phosphorylation modifications, we performed a comprehensive quantitative phosphoproteomics characterization of ccRCC tumor and normal adjacent tissues. Here, we identified 16,253 phosphopeptides, of which more than 9000 were singly quantified. Our in-depth analysis revealed 600 phosphopeptides to be significantly differentially regulated between tumor and normal tissues. Moreover, our data revealed that significantly up-regulated phosphoproteins are associated with protein synthesis and cytoskeletal re-organization which suggests proliferative and migratory behavior of renal tumors. This is supported by a mesenchymal profile of ccRCC phosphorylation events. Our rigorous characterization of the renal phosphoproteome also suggests that both epidermal growth factor receptor and vascular endothelial growth factor receptor are important mediators of phospho signaling in RCC pathogenesis. Furthermore, we determined the kinases p21-activated kinase 2, cyclin-dependent kinase 1 and c-Jun N-terminal kinase 1 to be master kinases that are responsible for phosphorylation of many substrates associated with cell proliferation, inflammation and migration. Moreover, high expression of p21-activated kinase 2 is associated with worse survival outcome of ccRCC patients. These master kinases are targetable by inhibitory drugs such as fostamatinib, minocycline, tamoxifen and bosutinib which can serve as novel therapeutic agents for ccRCC treatment.

Clear cell Renal Cell Carcinoma (ccRCC) is the most common (~75% frequency) and most malignant histological subtype of kidney cancer caused primarily by loss of the tumor suppressor von-Hippel-Lindau (*VHL*) gene (1). The disease accounts for more than 140,000 deaths worldwide every year (2) and is characterized by a 5-year survival rate of <10% for advanced tumors (3). Despite the increasing interest in understanding the pathogenesis of this cancer type, RCC is still mainly treated by surgical resection of the tumor mass as it is considered to be resistant to traditional chemotherapy and radiotherapy (2). In recent years, high-throughput mass spectrometry–based phosphoproteomics analysis of cancer biopsies has emerged as promising tool to elucidate the underlying molecular mechanisms of tumor pathology. Phosphorylation is the most common and most important reversible post-translational modification (4). It is assumed that around 75% of the human proteome is transiently phosphorylated in order to regulate and maintain biological processes such as cell division, protein synthesis, cell growth, apoptosis and development (4, 5). In fact, kinases, which are in many cases enzymes or receptors, are attractive targets for numerous Food and Dug Administration (FDA)-approved drugs (4, 6). However, attempts to portray the phosphorylation profile of ccRCC tumors are scarce. Deb *et al.* (7) conclude by comparing the respective Clinical Proteome Tumor Analysis Consortium (CPTAC) data that the ccRCC phosphoproteome is in general distinct from that of five other cancer types, as lower abundance levels for 161 common phosphosites were determined in RCC. Furthermore, the CPTAC phosphoproteome of ccRCC (8) includes more than 40,000 identified phosphosites detected by Fe^{3+}-immobilized metal affinity chromatography and represents, besides the study of Peng *et al.* (9), one of the largest phospho-profiles of ccRCC tissues. However, while the CPTAC analysis uncovered druggable phosphorylation signaling events such as the epidermal growth factor receptor

From the [1]Department of Molecular Biology and Genetics, Koc University, Istanbul, Turkey; [2]Department of Pathology, and [3]Department of Urology, Koc University School of Medicine, Istanbul, Turkey; [4]Department of Urology, Istanbul University, and [5]Department of Pathology, Istanbul University, Istanbul Faculty of Medicine, Istanbul, Turkey; [6]Koc University Research Center for Translational Medicine (KUTTAM), Omics Laboratory, Istanbul, Turkey

*For correspondence: Nurhan Ozlu, nozlu@ku.edu.tr.

https://doi.org/10.1016/j.mcpro.2022.100417

(EGFR)-mediated mitogen-activated protein kinase (MAPK) and AKT1-mTOR pathways, Peng *et al*. were rather interested in the general identification of missing proteins (evidenced only at the transcript level but predicted at the protein level). Another attempt described by Haake *et al*. (10) aimed to characterize tyrosine phosphorylations by pY-immunoprecipitation in ccRCC tissues and cell lines, respectively. Elevated tyrosine phosphorylation profiles were determined for the EGFR, MAPK as well as the focal adhesion kinase pathways in the different biospecimens, which can be effectively targeted by various tyrosine-kinase inhibitors (10).

Here, we performed dimethylation-based quantitative phosphoproteomics analysis of ccRCC tissues to illuminate previously undescribed signaling cascades. For the phosphopeptide enrichment, we employed on-column TiO_2-MOAC (metal oxide affinity chromatography) and detected more than 16,000 phosphopeptides. Our approach revealed that besides the MAPK and EGFR pathways, a vascular endothelial growth factor receptor (VEGFR)-induced pathway is strongly activated in the tumor tissues leading to the activation of multiple CDK and p21-activated kinases (PAK) kinases. Our findings suggest that these events drive tumor growth, progression and invasion.

EXPERIMENTAL PROCEDURES

Ethics Statement

The study proposal was approved by the Ethics Committee of Koc University in September 2017 (no. 2017.145.IRGB2.051) and was prolonged for two more years. Tissue samples were collected with the patients' informed written consent following the guidelines of the Declaration of Helsinki.

Sample Collection

The same tumor and matched normal adjacent tissue (NAT) samples of the discovery cohort from our previous publication were used for phosphoproteomics analysis (11). The age of the 13 patients varied between 47 and 74 and reflected a typical gender representation for RCC with a 1.6:1 male-to-female-ratio (supplemental File S1). Resected tissue samples were reached to the pathologist within 10 min and viable tumor areas were immediately sectioned and stored at −80 °C for subsequent pathological evaluation and proteomics sample preparation (supplemental Fig. S1).

Experimental Design and Statistical Rationale

For quantitative phosphoproteomics analysis, proteins from 13 frozen tumor and normal tissue biospecimens, respectively, were isolated and subjected to LC-MS/MS analysis. The order of sample preparation was randomized and independent of the patient list (supplemental File S1). The same processed peptide samples that were used for global proteome analysis in our previous publication (11) were used in this study for phosphoproteomics characterization. To prevent bias from the chemical labeling of peptide samples (dimethylation), the labeling was swapped for half of the patient samples. Phospho-enriched samples were analyzed as triplicates and the total set of identified phosphopeptides was subjected to multiple filtration steps to reduce the data into "high-confidence" (quantified in ≥75% of the cohort, Tier I) and "medium-confidence" (quantified in ≥50% of the cohort, Tier II) phosphopeptides. For comparative analysis, the obtained phosphopeptides were compared to different databases such as PhosphoSitePlus, CPTAC (ccRCC) and The Cancer Genome Atlas Kidney Renal Clear Cell Carcinoma (TCGA-KIRC), respectively. To determine significantly regulated phosphopeptides between tumor and normal tissues, one-sample Wilcoxon signed-rank test (p-value <0.05) was employed on the median $\log_2$ tumor/normal ratios.

In-Solution Digest, Isotopic Labeling and Fractionation of Samples

Sample preparation steps including protein digest, peptide labeling and fractionation are described in our previous study (11). Briefly, NAT and tumor tissue samples were subjected to protein isolation using a urea based lysis buffer followed by extensive homogenization in a bullet blender. Trypsinized samples were then labeled at their primary amines (N terminus and lysine residues) with heavy and light dimethyl isotopes to incorporate a fixed mass difference between sample types. Labeling reagents were swapped for half of the samples in order to prevent bias from the labeling choice (supplemental File S1). After mixing the labeled samples of a patient at 1:1 heavy-light-ratio, the peptide mixtures (estimated protein amount 1.2 mg) were fractionated on-column by strong cation exchange chromatography into 10 fractions. Desalted fractions were stored at −20 °C.

Phosphopeptide Enrichment

Enrichment of phosphopeptides was performed on-column by MOAC using 500 μg of titanium dioxide (TiO_2) beads (5 μm, Sachtleben) packed into microcolumns (20 μl GELoader, Eppendorf), which were equilibrated with loading buffer [80% acetonitrile (ACN) and 6% trifluoroacetic acid] (12). The dried desalted dimethyl-labeled peptide fractions were reconstituted in loading buffer to a final concentration of 1 μg/μl and the 10 fractions were pooled into six fractions. The peptides were slowly loaded onto the positively charged microcolumns at 50*g*. The bound phosphopeptides were washed with 0.1% trifluoroacetic acid in 50% ACN and then eluted with 20 μl of 10% ammonia solution into a new tube containing 35 μl of 10% formic acid (FA). The eluted peptides were further acidified by addition of 3 μl of 100% FA and immediately analyzed in LC-MS/MS.

Data Acquisition

The phospho-enriched fractions were analyzed in triplicate with a 120 min linear gradient on an UltiMate 3000 RSLCnano reversed phase chromatography platform (Thermo Fisher Scientific) coupled to a Q Exactive HF hybrid quadrupole-Orbitrap mass spectrometer (Thermo Fisher Scientific). The fractions were loaded onto an in-house packed 100 μm i.d. × 17 cm C18 column (Reprosil-Gold C18, 5 μm, 200 Å, Dr Maisch) and run with a flow rate of 300 nl/min. The chromatographic separation of the peptides started at 4% of solution B (ACN with 0.1% FA) and gradually increased to 25% in 67 min. The gradient continued from 25% to 45% of solution B in the next 20 min. Peptides in the mass range of 400 – 1,500 m/z and with a positive polarity were allowed for detection in data-dependent mode. For the MS1 spectra acquisition, the resolution was set to 120,000, the automatic gain control (AGC) target to 1e6, and the maximum injection time to 60 ms. The top 20 most intense peptides per cycle were selected for fragmentation in the higher-energy collisional dissociation cell with a normalized collision energy of 27. MS2 spectra acquisition was conducted at a resolution of 30,000, an AGC target of 1e5, a maximum injection time of 60 ms, and a fixed first mass of 100 m/z. Furthermore, the isolation window was set to 2.0 m/z, the dynamic exclusion to 20 s, the minimum AGC to 3e3, and the charge exclusion was set as unassigned, 1.

Data Processing

Peptide identification and quantification from raw MS data files were done with Proteome Discoverer (PD) (v1.4, Thermo Scientific)

using the Mascot (v2.5.1, Matrix Science) search engine. The peptide spectral matches were searched against a Swissprot database containing 21,039 entries for *Homo sapiens* retrieved from Uniprot in March 2016. Trypsin was selected as hydrolytic enzyme with a maximum number of allowed missed cleavages of two. For peptide identification, a mass tolerance of ±20 ppm for precursor masses and ±0.05 Da for fragment ions was selected. For dimethyl labeling, the 2plex dimethyl-based heavy/light quantitation method with a mass precision requirement of 2 ppm for precursor ions was used. Light and heavy dimethylation of peptide N termini and of lysine residues, phosphorylation at serine, threonine and tyrosine residues, as well as methionine oxidation were set as dynamic modifications. Cysteine carbamidomethylation was set as fixed modification. Determination of phosphosite positions was done by using the implemented node phosphoRS (v3.0). The false discovery rates (FDR) for peptide and protein identifications were set to 1% using the Percolator node in PD (13). Furthermore, a filter was applied to allow only peptide identifications with medium and high confidence, with a sequence length between 7 and 25, a Mascot score >20 and a peptide rank of 1.

Quantification ratios of samples with swapped dimethyl labeling were converted to tumor/normal format. The data were filtered for peptides quantified in at least two out of three technical replicates in any of the 13 biological replicates. The 3810 resulting phosphopeptides are hereafter denoted as "quantified phosphopeptides". A second filter was applied to reduce the data to phosphopeptides quantified in ≥75% of the cohort (Tier I) or ≥50% of the cohort (Tier II). All quantification ratios were then normalized to the median of the non-phosphorylated peptides in the sample and $\log_2$ transformed. The phosphorylated peptides were further filtered for ≥50% phosphosite probability.

For statistical analysis, the Python function scipy.stats.wilcoxon (v0.14.0) was extended by the feature to omit missing quantification values and was then applied peptide-wise on the whole technical replicates data. *p*-values <0.05 were considered statistically significant which led to a total of 600 (Tier I) and 1,223 (Tier II) "significantly regulated phosphopeptides", respectively. All subsequent analyses were performed with the Tier I dataset unless otherwise stated.

For the determination of statistical difference between phosphopeptide and non-phosphopeptide distributions, two-sample Student's *t*-test (*p*-value <0.05) was applied via the Python function scipy.stats.ttest_ind.

Functional Annotation

Significantly up-regulated and down-regulated phosphorylated proteins were annotated by their Gene Ontology biological process association using the PANTHER (v14) platform (14) with an FDR setting of 0.05. The proteins were further annotated by their function in cancer using the COSMIC Cancer Gene Census database (v91) (15) and also by associated FDA-approved drugs with inhibitor function retrieved from the Drugbank database (v5.1.7, access August 2020) (16). Chemical elements were excluded as drugs.

To further characterize the functionality of the phosphopeptides, a previously published study from our group on the epithelial-to-mesenchymal phosphoproteome (17) was used for sequence-based comparison with the determined significantly dysregulated phosphopeptides.

Moreover, we assessed for the significant phosphopeptides the probability of biological relevance by using the data of Ochoa *et al.* (18) and by annotating the phosphopeptides with their reported functional score. More specifically, both datasets were matched by the protein sequence position and the residue type of the modification. Only phosphopeptides with a score >0.5 were considered functional.

Kinase-Substrate Network Recreation

To predict kinase activities in the tumor and NATs, we implemented the NetworKIN3.0 (19) algorithm (access August 2022), which annotates kinases based on STRING interactions and phylogenetic links within kinase families. For this purpose, the significantly regulated phosphopeptides of the Tier II dataset were centered to their phosphosite and expanded by the surrounding ±7 amino acid (aa) sequence window. Only kinase-substrate predictions with a NetworKIN score >5 were considered for network recreation using the visualization software Cytoscape (v3.8.0). The network components were annotated by their Gene Ontology cellular compartment feature using QuickGO (20), limited only to Uniprot assignments. In case of multiple cellular allocations, priority was given as follows: "membrane", "nucleus", "cytoplasm", "extracellular" and "other", respectively. Additionally, the recreated network was complemented with the enriched Reactome pathways retrieved as over-representation analysis of the kinases and substrates via the webtool WebGestalt (v2019) (21) (access August 2022) at default settings.

The predicted kinases were further mapped to the human kinome phylogenetic tree using the $\text{KinMap}_{\text{beta}}$ tool at www.kinhub.org (access August 2022) (22).

Motif and Survival Analysis

To find conserved sequence motifs, the ±7 aa sequence windows of the centered significantly regulated phosphosites were subjected to the webtool MoMo (v5.3.3) (23) (access August 2022), which applies the motif-x algorithm. For the predictions, a 15 residue motif width, 20 occurrences, and a *p*-value of <0.000001 were set.

For the determination of the prognostic power of kinases, the web tool Kaplan–Meier Plotter (24) (access August 2022) was used with the mRNA data of the TCGA-KIRC cohort (n = 530) (25) and the "auto select best cut-off" option to optimally partition the patients based on the lowest *p*-value and the highest hazard ratio.

Additionally, the proteome data of the CPTAC cohort (n = 102) (8) was used for survival analysis. For this purpose, the CPTAC global proteome and phosphoproteome data were processed by removing control samples, non-ccRCC samples and contaminated samples, respectively. Furthermore, the phosphopeptide data were aggregated to obtain phosphoprotein quantification values by calculating the mean abundance value from all quantified phosphopeptides of a protein in a sample. Individual tumor quantification values were then gene-wise normalized to the median quantification value of all normal tissue samples. Partitioning of the CPTAC cohort into "low and high expression" was based on the mean quantification value of the kinase of interest as cut-off. Survival curves were created using the KaplanMeierFitter and multivariate_logrank_test functions of the Python library lifelines (v0.25.0).

Comparison With Omics Data

The generated phosphoproteomics data were compared with the corresponding global proteome data of the same tissue samples previously described by our group (11). More specifically, the median $\log_2$ tumor/normal ratio for a given phosphopeptide was compared with the respective ratio of the available non-phosphorylated version of the peptide.

The identified phosphosites of this study were also compared with the PhosphoSitePlus database (access November 2020) (26) by matching the ±7 aa sequence windows. We further compared our ccRCC phosphoproteome with the processed CPTAC data (8) by matching protein sequence positions of identified individual phosphosites. Furthermore, the phosphosite datasets were also compared quantitatively by their median $\log_2$ tumor/normal ratios (CPTAC cohort with both tumor and matched normal tissue samples, n = 80). Pearson

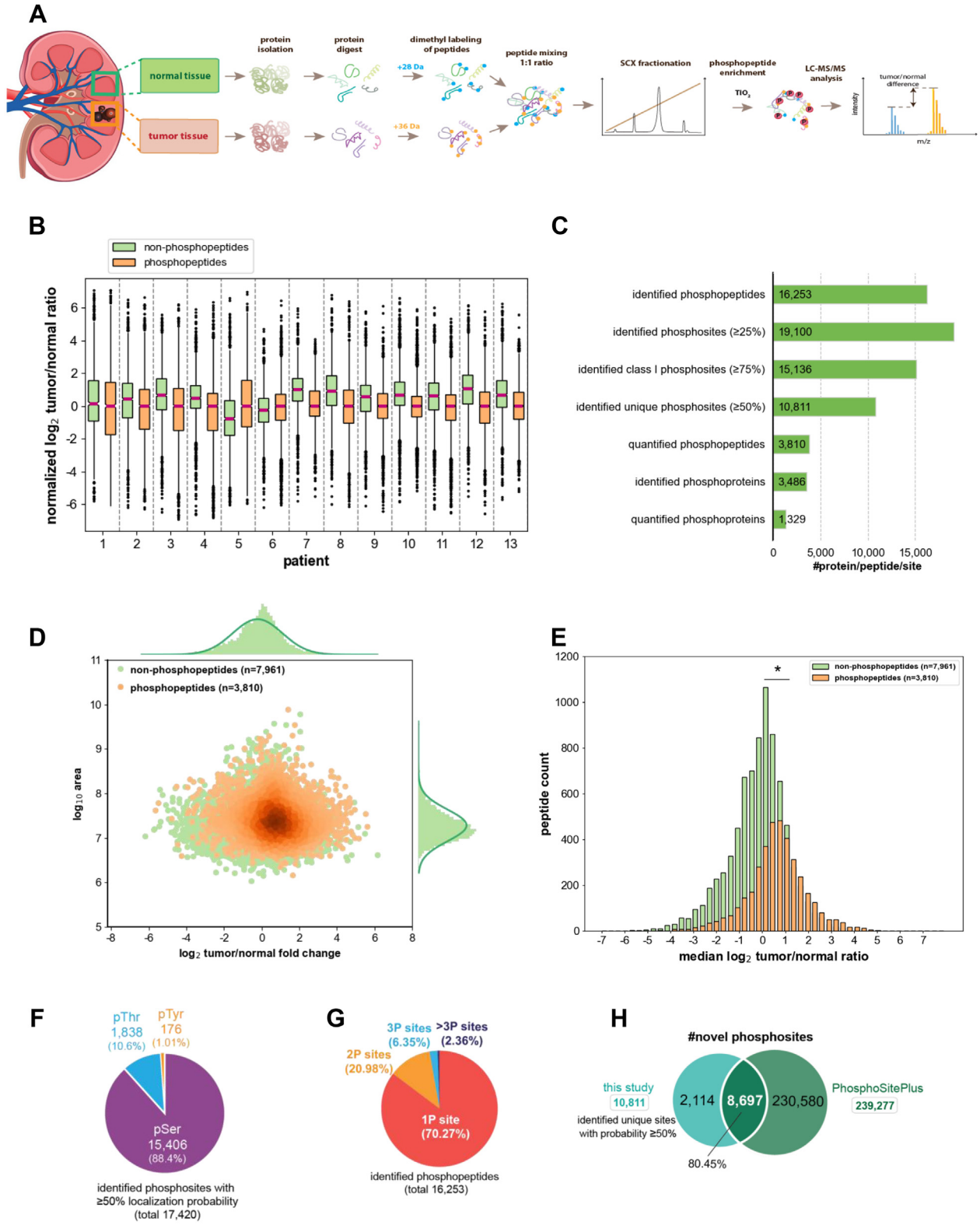

FIG. 1. **Phosphoproteome analysis of clear cell Renal Cell Carcinoma**. *A*, experimental outline of dimethylation-based quantitative phosphoproteomics approach. *B*, distribution of quantified phosphopeptides and non-phosphopeptides across all patients. *C*, number of identified and quantified phosphopeptides and phosphoproteins. "Quantified" refers to quantifications in at least two out of three technical replicates. *D*, MA plot depicting intensity distribution of quantified phosphopeptides and non-phosphopeptides. Top and right histograms show

and Spearman correlations were calculated for common quantified phosphosites using the respective Python scipy.stats functions.

Cell Viability Assay

Approximately 7500 cells (CAKI-2, A498 and MCF7) were seeded in 96-well cell culture plates and treated with different concentrations of tamoxifen (25–100 μg/μl) for up to 72 h. After each 24-h treatment with the drug, the cells were fixed with 50% trichloroacetic acid for 1 h at +4 °C. Viable cells were stained for 30 min at room temperature using 0.4% sulforhodamine B solution and washed with 1% acetic acid. 10 mM Tris solution was then added to the wells and the optical density was measured at 564 nm in a Thermo Scientific MultiskanGO plate reader. For each individual experiment, cell survival changes were expressed as percent of the untreated control. Statistical analysis was done using two-way ANOVA in GraphPad PRISM v9.

RESULTS

Shotgun Proteomic Approach Achieves Deep Coverage of ccRCC Phosphoproteome

In this study, a comprehensive quantitative phosphoproteomics analysis of frozen ccRCC tumors and NATs has been conducted to illuminate undiscovered signaling pathways mediated by protein phosphorylation. For this purpose, the dimethyl-labeled fractionated peptides of tumor and NATs from our previous global proteomics analysis (11) were subjected to phosphopeptide enrichment using TiO_2 beads and were analyzed as technical triplicates in LC-MS/MS (Fig. 1*A*). The discovery cohort consisted of 13 patients of different age, grade, stage and gender. In general, the identification and quantification of phosphorylated and non-phosphorylated peptides in the enriched samples were robust across patients and spanned approximately 12 orders of magnitude in the tumor/normal fold change dynamic range (Fig. 1*B*). In total, we identified 16,253 phosphopeptides from the tumor and NAT samples with an FDR of 0.01, which were assigned to 3486 phosphoproteins (Fig. 1*C*). The majority of the identified phosphosites (15,136) were class I sites with a localization probability of ≥75%. Out of these phosphosites, 10,811 were unique sites (localization probability cut-off ≥50%). Furthermore, 3810 dimethyl-labeled phosphopeptides were quantified in both tumor and NATs, which corresponded to 1329 quantified phosphoproteins. In general, the abundance levels of quantified peptides (log_{10} peak area) varied over 4 orders of magnitude in dynamic range (Fig. 1*D*). Moreover, the fold change distributions of quantified phosphopeptides and non-phosphopeptides followed a near normal pattern (Fig. 1*D*, top histogram), however, a significant skewness of phosphopeptide ratios toward positive values was noticeable suggesting enhanced phosphorylation events in the tumor tissues compared to NATs (Fig. 1*E*). As expected, most phosphosites were serine residues (88.4%), followed by threonine (10.6%) and tyrosine residues (1.01%) coinciding with previously reported frequencies (4) (Fig. 1*F*). Furthermore, most peptides were singly phosphorylated (70.3%), while only a small portion of peptides harbored multiple phosphosites, which is also in line with previous observations (9) (Fig. 1*G*). Comparing the identified phosphopeptides of this study with the PhosphoSitePlus database revealed that approximately 80.5% were already reported, implicating that the majority of phosphorylation modifications in kidney cancer are not tissue-specific (Fig. 1*H*).

Significantly Regulated Phosphorylations Play a Role in Tumor Invasion and Harbor Conserved Kinase Recognition Sites

Out of more than 3810 quantified phosphopeptides, we determined 600 as statistically differentially abundant between tumors and NATs (Wilcoxon signed-rank test, p-value <0.05) (Fig. 2*A*), which were assigned to 323 unique proteins (supplemental File S2). The majority were up-regulated phosphopeptides (Fig. 2, *A* and *B*), supporting our observation of elevated phosphorylation events in ccRCC tumors (Fig. 1*E*). Interestingly, the 269 significantly up-regulated phosphoproteins in the tumors were primarily associated with protein synthesis and cytoskeleton organization, while the 60 significantly down-regulated phosphoproteins were associated with actin-filament organization (Fig. 2C). These aberrant biological processes suggest an increase in cell growth, cell motility and invasiveness, which are indicators of malignant tumors and have previously been linked to worse patient outcome (27). Among the phosphorylated intermediate filament components were vimentin (supplemental File S2 (Tier I & Tier II)) and several keratins (KRT) such as KRT8 (supplemental Fig. S5, *A* and *B* and supplemental File S2 (Tier II)) and KRT19 (supplemental File S2 (Tier II)).

To further understand the effect of phosphorylation, we compared the generated phosphoproteome profile with our global proteome data of the same ccRCC tissues (Fig. 2, *D–F*) (11). The majority of the 323 dysregulated phosphoproteins (76.5%) were not significantly regulated at the global proteome level, while 76 phosphoproteins (23.5%) were also significantly regulated on the global level (Fig. 2, *D* and *E*). This implies that most of the phosphorylated proteins are similarly abundant between tumor and normal tissues and that the generally low stoichiometry of the phospho-proteoforms is sufficient for molecular impact in the tumor cells such as

distribution of fold change values and intensities of non-phosphopeptides, respectively, with density lines representing theoretical normal distribution. *E*, histogram showing general distribution of median tumor/normal ratios of quantified phosphopeptides and non-phosphopeptides. *Student's *t* test was applied for statistical determination of skewness between distributions, p-value <0.05. *F*, frequency distribution of identified serine (pSer), threonine (pThr) and tyrosine (pTyr) phosphosites with ≥50% localization probability. *G*, frequency distribution of identified singly (1P site) and multiply (≥2P sites) phosphorylated peptides with ≥50% site probability. *H*, comparison of identified phosphosites with ≥50% localization probability with PhosphoSitePlus database. ccRCC, clear cell Renal Cell Carcinoma.

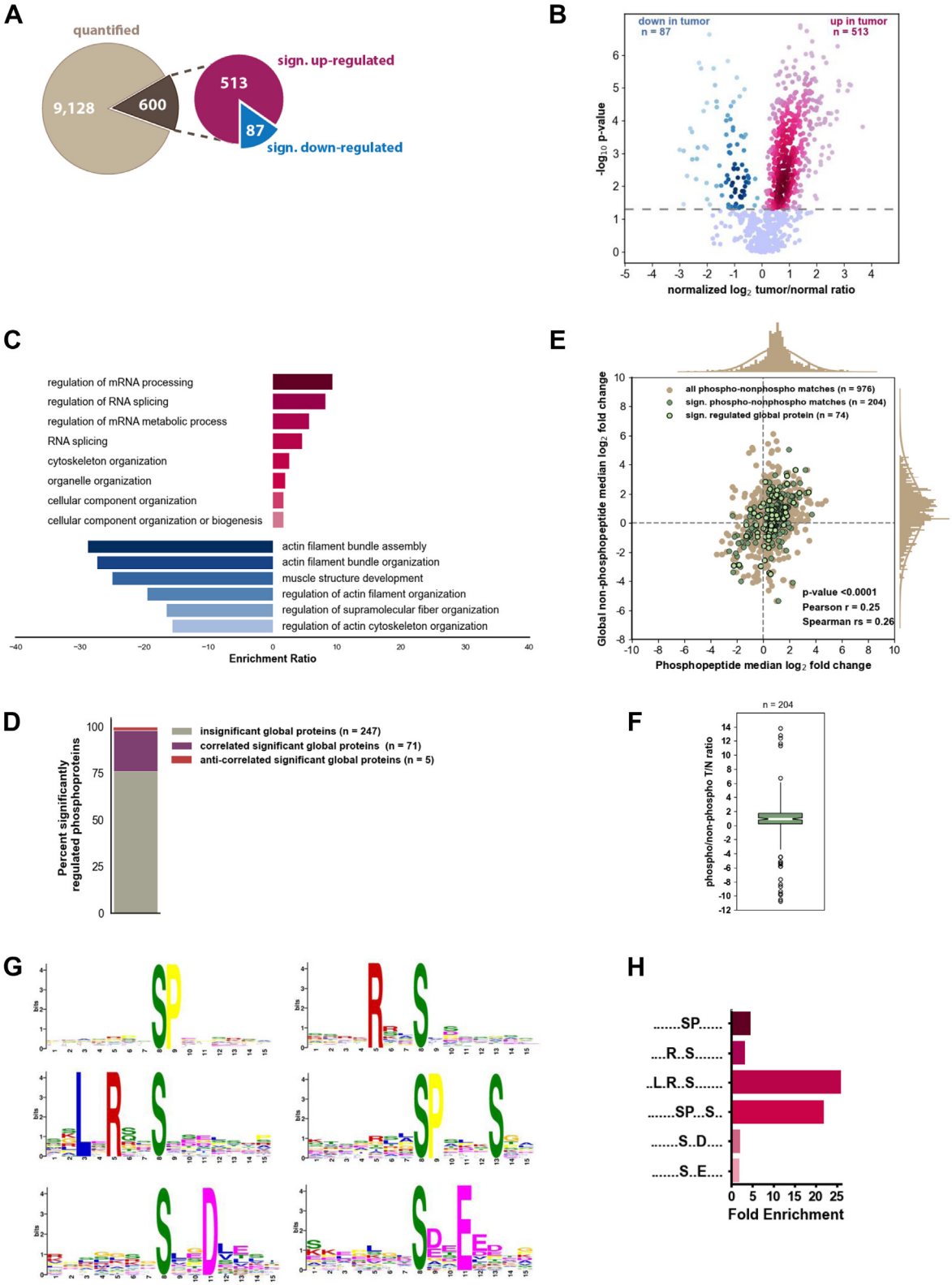

FIG. 2. **Significantly regulated phosphorylations in ccRCC**. *A*, overview of the number of quantified phosphopeptides. Inner pie chart represents number of significantly regulated phosphopeptides with the majority being up-regulated in the tumor tissues. *B*, volcano plot depicting significantly regulated phosphopeptides. *C*, enriched biological processes in ccRCC tumors compared to adjacent normal tissues. Top 10 PANTHER GO-Slim biological process annotations of significantly up-regulated (*pink*) and down-regulated (*blue*) phosphoproteins,

change in the activity, structure, conformation or localization of proteins (28). To assess whether the phosphorylation modification itself or the general abundance of the peptide was elevated in the tumors, we compared for the 600 significantly regulated phosphopeptides the abundance levels between the phospho and available non-phosphorylated version (Fig. 2*F*). In total, 204 of the 600 significantly regulated phosphopeptides had a non-phosphorylated counterpart in the global proteome. Indeed, the $\log_2$ tumor/normal ratios of phosphorylated peptides were significantly higher compared to those of the respective non-phosphopeptides (Wilcoxon signed-rank test, *p*-value <0.00001) (Fig. 2*F*), confirming that the observed signaling events are due to phosphorylation of the proteins.

Furthermore, 296 of the 513 significantly up-regulated phosphopeptides were associated with conserved serine recognition sequences (Fig. 2, *G* and *H* and supplemental File S4) such as the proline-containing serine motifs xxxxxxxSPxxxSxx and xxxxxxxSPxxxxxx, which are known target sites of the mitotic kinases cyclin-dependent kinase 1 (CDK1) and CDK5, respectively (29). Other frequent kinase target motifs were xxLxRxxSxxxxxxx and xxxxRxxSxxxxxxx, which are associated with different kinase groups such as CaMK, AMPK, PKA and PKCα, respectively (29).

CDK1 and PAK2 Kinases Are Highly Activated in ccRCC Tumors

In order to unveil the most prominent kinase activities, we applied the kinase prediction tool NetworKIN on the determined significantly regulated phosphosites (600 in total, see Fig. 2, *A* and *B*). We reduced the predictions to high-confident ones with a NetworKIN score of ≥5 (178 predictions in total). In summary, out of the 323 significantly regulated phosphoproteins, 82 were substrates of a total of 53 different kinases (supplemental File S4). Among the most frequently activated kinases were different CDK kinases such as CDK1 and CDK5 (Fig. 3*A*), which confirms our previous finding that the conserved phosphosite recognition sequences of these kinases are highly enriched (Fig. 2, *G* and *H*). Furthermore, p21-activated kinase 2 (PAK2) is the second most activated kinase in the tumor tissues, followed by GSK3β and c-Jun N-terminal kinase 1 (JNK1) (Fig. 3*A*). Also, predictions for the kinases p38β (MAPK11) and p38γ (MAPK12) are highly enriched and suggest the activation of the MAPK pathway (8). In contrast, the activity for the kinases TGFbR2, AKT1, PAK1, CaMK2γ as well as PDHK2 and PDHK3 was reduced in the tumor tissues compared to NATs. Furthermore, all predicted kinases belonged to serine/threonine families (Fig. 3*B*). The majority of the kinases belonged to the CMGC, AGC and STE families with an overall increased activity in the ccRCC tumors (supplemental Fig. S2*C*). Moreover, the rare kinase family PDHK was only associated with reduced phosphorylation events in the tumors.

To illuminate the most prominent signaling pathways in the ccRCC tumors, we recreated the predicted kinase-substrate interactions as network and complemented it with the associated Reactome pathways (Tier II data, Fig. 3*C* and supplemental File S4), which unveiled that certain malignant processes such as AKT signaling, VEGF signaling, MAPK-related signaling, and signaling by interleukins and second messengers shape the pathobiology of renal cancers. Moreover, the activation of RAC1 is the most enriched pathway in the tumors, with all known six PAK kinase isoforms predicted to be activated in the tumors (PAK1 and PAK4 are also associated with down-regulated phosphopeptides, supplemental File S4). We further annotated the genes in the network by their role in cancer (colored font) and noticed that several known oncogenes are substrates of the kinases such as EGFR, MAPK1, AKT1, AKT2, MAP2K1, MAP2K2, SGK1, BRAF and CDK4. Furthermore, nine substrates were identified to have a mesenchymal phosphorylation (yellow border) (17) such as PKCi, CHAMP1, BCKDK, MYEF2, PRCKa and PLEC, among others (supplemental File S4).

Functional Phosphorylation Events Are Targetable by FDA-Approved Drugs

Given that identified phosphorylations might be functionally redundant or non-functional (5, 18), we sought to unravel those most likely to contribute to tumor pathobiology. To this end, we compared our phosphopeptide data with the functionality analysis of Ochoa *et al.* (2020) (18) and determined that out of the 600 significantly regulated phosphopeptides, 230 are most likely functional (score >0.5) (supplemental Fig. S2*D*). Next, we annotated the functional up-regulated phosphopeptides by their predicted kinases to find the most relevant kinases in renal cancer (Fig. 4*A*). This revealed that CDK1, PAK2, p38γ (MAPK12), JNK1 and p38β (MAPK11) are the kinases responsible for most of the functional phosphorylations in ccRCC tumors (Fig. 4*A* and supplemental File S4). Since kinases are the major targets for cancer drugs (6), we further annotated the predicted kinases by their inhibitory

respectively. *D*, corresponding regulation of significantly regulated phosphoproteins in global proteome of same ccRCC tissues as described in (11). *E*, scatter plot depicting distribution of matching phosphopeptides with non-phosphorylated counterpart of global proteome. Indication of matches associated with significant protein abundance changes in global proteome in light green. *F*, tumor/normal fold change distributions of significantly regulated phosphopeptides with respective non-phosphorylated counterpart. For statistical evaluation of distribution, BH-adjusted *p*-value correction was applied after one-sample Wilcoxon signed-rank test. *G–H*, enriched consensus motifs of significantly regulated serine and threonine phosphopeptides sorted by their ascending *p*-value (gradient coloring). Phosphosites with ≥50% probability (centered to the phospho residue and enlarged by the ±7 aa sequence window) were used for the analysis with the motif-x algorithm. ccRCC, clear cell Renal Cell Carcinoma.

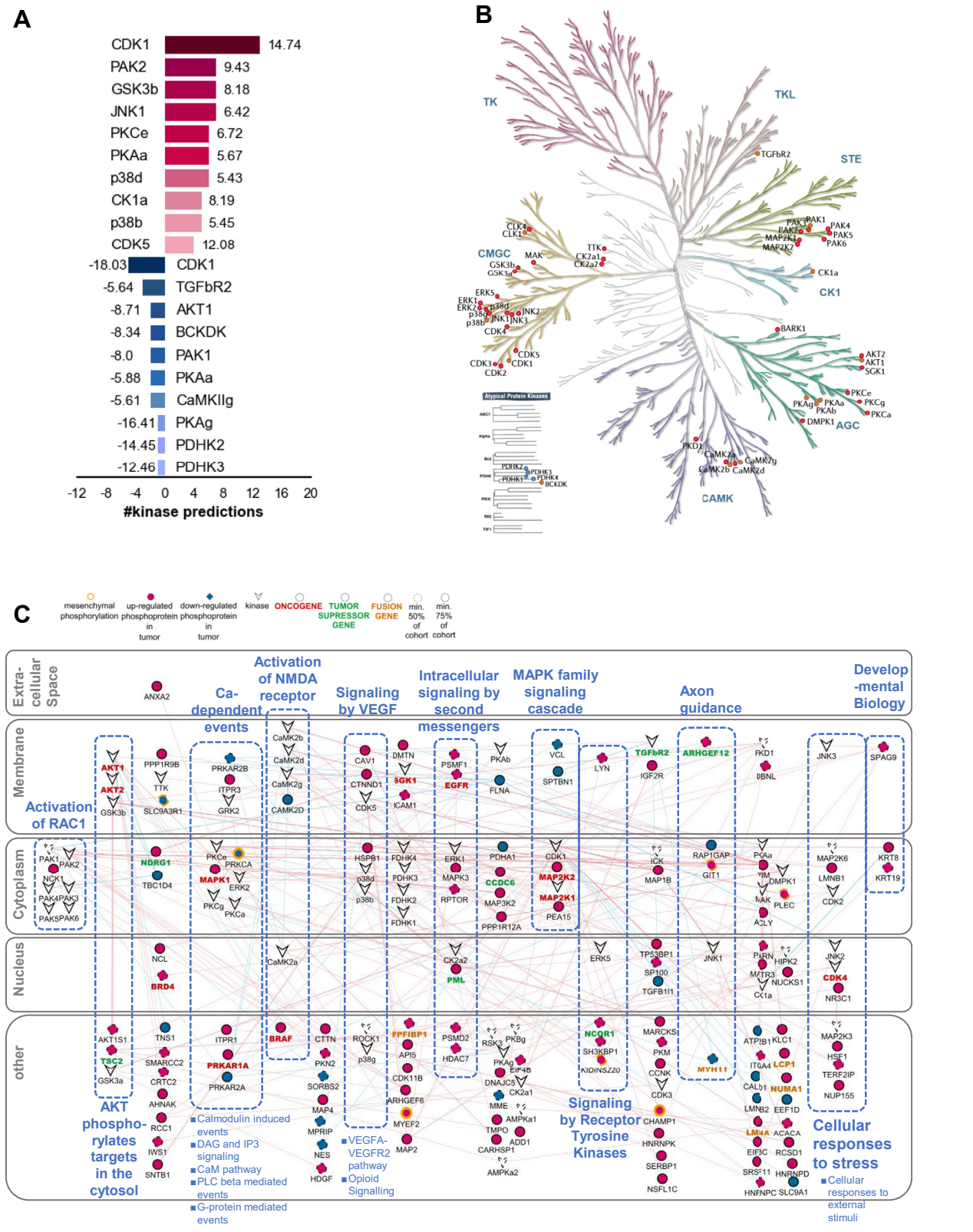

FIG. 3. **Altered kinase activities in ccRCC tumors**. *A*, predicted activated and reduced kinases in the tumor tissues compared to NATs according to the NetworKIN3.0 tool. Top 10 kinases with highest number of predictions are shown (with gradient coloring representing ranking). Average NetworKIN scores of predictions are shown as bar labels. *B*, human kinome tree of activated and reduced kinases in ccRCC tumors.

FDA-approved drugs. Indeed, approximately 77% of the activated kinases (41 out of 53) are druggable (supplemental Fig. S2*E*). A subnetwork for the three most relevant kinases with the indication of functional phosphorylations (black font) is shown in supplemental Fig. S5*A*. While PAK2 and CDK1 can be targeted by the tyrosine kinase inhibitor fostamatinib, JNK1 can be inhibited by tamoxifen and minocycline. Furthermore, cell viability assays showed for tamoxifen (supplemental Fig. S5*E*), which targets besides JNK1 several PKC kinases (supplemental File S4), a significant toxic effect on CAKI-2 as well as A498 cells at low concentrations (p-value <0.05). Both kinase groups were previously reported to increase proliferation and invasiveness of ccRCC cells (30, 31). Tamoxifen is widely used for breast cancer treatment (32) and our results support the efficacy of this drug for ccRCC as a similar cell viability was determined between A498 cells and MCF7 cells (supplemental Fig. S5*E*). Moreover, 22 out of the 53 kinases in Figure 4*A* have a prognostic value for ccRCC tumors based on TCGA-KIRC follow-up data (n = 530 patients) including several CDKs such as CDK1, CDK2, CDK3, CDK4 and CDK5, as well as several MAPKs such as MAPK11, MAPK13, MAPK7 and MAP2K2 (supplemental Fig. S3), which stresses the importance to investigate cell proliferation–related pathways. Furthermore, CPTAC follow-up data showed for PAK2, CDK4, PKCa and CLK4 significantly worse survival outcome (log-rank test, p-value <0.05) for the global proteome supplemental Fig. S4*A*) and phosphoproteome data (supplemental Fig. S4*B*) of ccRCC patients, respectively, due to high expression of these kinases in the tumor tissues compared to NATs.

A summary of the most elevated signaling pathways orchestrated by phosphorylation in ccRCC tumors and relevant kinase inhibitors is illustrated in Fig. 4*B*.

DISCUSSION

In this study, we identified 16,253 phosphopeptides on 3486 proteins by quantitative phosphoproteomics analysis of ccRCC tissues and NATs (Fig. 1*C*). Comparison with other high-throughput approaches to characterize the ccRCC phosphoproteome revealed a high level of concordance between our study and the CPTAC phosphoproteome (supplemental Fig. S5, *B* and *C*). Approximately 66% of the identified phosphosites of this study are shared with the CPTAC dataset. In total, 6775 quantified common phosphosites displayed a significant positive correlation (0.54, p-value <0.05, supplemental Fig. S5*C*) between both datasets. More than 3700 phosphosites are unique to our study suggesting previously undescribed observations of phospho signal transduction in ccRCC such as ion homeostasis, microtubule polymerization/depolymerization, protein localization, wound healing and cell–cell junction assembly (supplemental File S2). These phosphosites might have been caught due to the different phosphopeptide enrichment method, as we applied TiO_2-MOAC based enrichment, while the CPTAC group used Fe^{3+}-immobilized metal affinity chromatography.

Our in-depth proteomics analysis predicted all six members of PAKs to be highly activated in the ccRCC tumors (Fig. 3*C*). PAKs are known to be switched on by the small GTPases Rac1 and Cdc42, and to be crucial for cytoskeletal dynamics, invasion, metastasis, cell death and proliferation (33). Previous phosphoproteomics studies have not described PAKs as relevant kinases in ccRCC tumorigenesis yet (8–10), however, our data strongly indicate that especially PAK2 is highly functional in the tumors as it is predicted to phosphorylate 13 functional peptides across seven different substrates (Tier II, supplemental Fig. S5*A*). In addition, PAK2 is one of the few kinases that has also been experimentally detected by our proteomics approach (supplemental Files S2 and S3), supporting its predicted elevated activity. While especially the role of PAK1 is largely understood in different cancers, the function and targets of PAK2 remain to be elucidated (33, 34). Furthermore, PAK2 has previously been noted to bind to CDK12, and thereby to activate the MAPK pathway (34). Our study shows for CDK1 and CDK5 high activity (Fig. 3*A*), which warrants further investigation to shed light into the synergistic functionality of PAKs and CDKs regarding cell cycle regulation in RCC. Moreover, both PAKs and CDKs have been linked to hypoxia, which is one of the main characteristics of ccRCC tumors (11, 35). More specifically, increased levels of PAKs are caused by hypoxia-induced activation of the mediators Rac1 and Cdc42 through phosphatidylinositol 3 kinase and protein tyrosine kinase (Fig. 4*B* and (36)). In contrast, CDKs are indirect downstream effectors of hypoxia as they are interactors of the hypoxia-induced cell cycle proteins cyclin D1, cyclin A and cyclin E, respectively (37). Furthermore, we determined for PAK5, PAK6, CDK1, CDK2, CDK3, CDK4 and CDK5 worse survival outcome at high expression levels based on TCGA-KIRC mRNA data (supplemental Fig. S3). Additionally, survival analysis based on both CPTAC proteome as well as phosphoproteome data revealed that PAK2 has a prognostic value for ccRCC patients (supplemental Fig. S4). Moreover, our analysis suggests that all PAKs can be inhibited by the tyrosine kinase inhibitor fostamatinib (Fig. 4*B*). It is worthwhile to examine the efficacy of fostamatinib in ccRCC

The web tool KinHub was used with indications of predicted kinases associated with significantly up-regulated (*red*), both up-regulated and down-regulated (*orange*), and down-regulated (*blue*) phosphopeptides, respectively. *C*, kinase-substrate network depicting the most enriched Reactome pathways (Tier II data). Nodes are organized by their cellular compartment retrieved using the QuickGO web tool. Enrichment level of pathways decreases from left to right. Mesenchymal phosphorylations (*orange border*) as well as the role of substrates in cancer (*node font color*) are also indicated. Incomplete node border indicates Tier II (quantified in ≥50% of cohort), while complete node border refers to Tier I (quantified in ≥75% of cohort). ccRCC, clear cell Renal Cell Carcinoma; NAT, normal adjacent tissue.

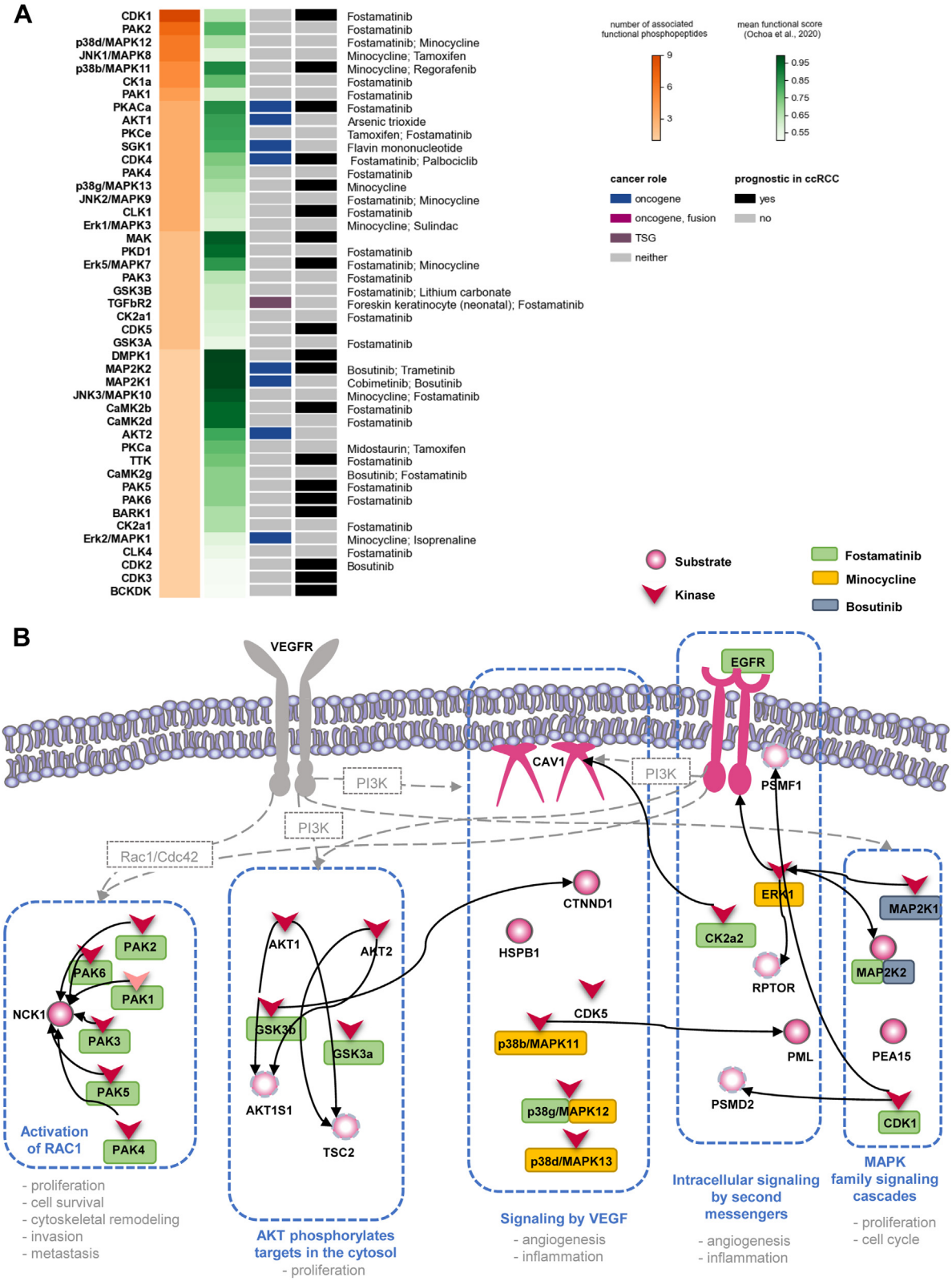

FIG. 4. **Altered kinase activities in ccRCC tumors.** *A*, predicted activated kinases associated with significantly up-regulated phosphopeptides with a functional score >0.5 according to Ochoa *et al.* (2020). Indicated drugs are associated FDA-approved therapeutics with inhibitor function (for complete drug list see supplemental File S4). The prognostic feature of the kinases refers to supplemental Fig. S3. *B*, summarized

treatment along with inhibitors for other signaling components such as CDKs and MAPKs as combinatorial anticancer strategy.

Another highly up-regulated phosphoprotein in the tumor tissues is the receptor tyrosine kinase EGFR. We have already described the potential involvement of the oncogenic EGFR-MAPK and EGFR-AKT1-mTOR axes, which are known to drive proliferation, inflammation, survival and metastasis, in our global proteome analysis of the same tissue samples (8, 11). EGFR has been reported to be overexpressed in RCC tumors, however, no clinically approved drug against EGFR is currently in use for RCC treatment (8, 10). Our data suggest that EGFR is a substrate of different predicted kinases such as PDK1, MAPK1, MAPK3, GRK2, CaMK2α and CaMK2γ (Tier II, supplemental Fig. S5*D*). We identified two significantly up-regulated phosphosites for EGFR, namely T693 and S1166, which are predicted to be functional modifications. EGFR is particularly known to be activated by tyrosine phosphorylations in its tyrosine kinase domain (713–965 aa) (supplemental Fig. S5*D*) (4); however, we could not detect sites in this domain, probably due to the intrinsic nature of our enrichment method to primarily catch serine and threonine residues. Based on our findings, we propose that both the experimentally derived EGFR-mediated pathways, as well as the predicted VEGFR-mediated signaling cascades are likely to synergistically govern malignant phospho signaling in ccRCC tumors (Fig. 4*B*).

As indicated by our data, the hyperphosphorylation of intermediate filaments such as vimentin or keratins is a major event in ccRCC tumors (Fig. 3*C* and supplemental File S2), which further supports the suggested migratory behavior of renal cancers (27, 38). It has been previously described that the levels of vimentin are four times higher in ccRCC, while the epithelial marker E-cadherin is expressed at half or only one third of the level compared to five other cancer types (7). This may provide a possible explanation for the fact that around one third of ccRCC patients already display distant metastasis at diagnosis (7). As with other epithelial carcinomas, keratins are also used as biomarkers for the accurate classification of renal cell carcinomas (39). ccRCC tumors mainly express KRT7, KRT8, KRT18 and KRT19 (39). Our analysis identified multiple up-regulated keratin phosphorylation sites, including KRT8 and KRT19, in ccRCC tumors (Tier II). These phosphorylated proteoforms of keratins may serve as valuable biomarkers in immunohistochemistry for subclassification of renal cancers.

Overall, our comprehensive phosphoproteomics profiling of ccRCC tissues shed new light on the signaling cascades driving renal tumorigenesis. Current approved treatment regimes for advanced tumors use the tyrosine kinase inhibitors sunitinib, pazopanib, cabozantinib, axitinib and sorafenib against VEGFR in the first-line setting (40). Furthermore, recent trials combining tyrosine kinase inhibitors with immunotherapeutics such as axitinib with pembrolizumab or with avelumab showed better toleration and median survival outcome than monotherapies (40). However, many trials have failed to effectively target other important mediators of RCC tumorigenesis such as EGFR (8, 10), which is also supported by our data to be a central player alongside VEGFR. Hence, future directions warrant the investigation of new targeted therapies against EGFR and its downstream effectors PAK and CDK kinases with the suggested agents fostamatinib and minocycline, also as combinatorial treatments with approved EGFR agents such as dacomitinib, cetuximab and erlotinib.

DATA AVAILABILITY

This article contains supplemental data. The mass spectrometry proteomics data have been deposited to the ProteomeXchange Consortium via the PRIDE (41) partner repository with the dataset identifier PXD028428.

Supplemental Data—This article contains supplemental data (8, 11, 18)

Acknowledgments—We gratefully acknowledge the KUPAM and KUTTAM OMICS facilities of Koc University, especially Busra Akarlar and Nazli Ezgi Ozkan Kucuk for their technical support. We thank Ozgur Kurt from Koc University School of Medicine for his essential help in pathological assessment of tissue samples, and Isin Kilicaslan and Yasemin Ozluk from Istanbul University Istanbul Faculty of Medicine for their supervisory contribution during pathological assessment of tissue samples. The results shown here are in whole or part based upon data generated by the TCGA Research Network: https://www.cancer.gov/tcga. Data used in this publication were generated by the Clinical Proteomic Tumor Analysis Consortium (NCI/NIH). NO acknowledges the Royal Society Newton Advanced Fellowship (NA170389).

Author Contributions—A. S. and N. O. designed the research plan. A. S. performed proteomics experiments, statistical analysis, data analysis and data visualization. A. T. S. performed cell viability assay and related data visualization. A. A. performed H&E staining of tissue samples. S. B. performed pathological assessment of tissues. O. A., M. C. K., S. E., A. A. and T. E. consulted on clinical questions. N. O. conceived and supervised the study. A. S. wrote the manuscript with inputs from N. O. and A. T. S. All authors discussed the results and commented on the manuscript.

significantly enriched phosphorylated pathways in ccRCC tumor tissues targetable with FDA-approved drugs (Tier II data). Enrichment level of pathways decreases from left to right. Signaling events that are predicted according to literature are shown in gray. Tier II nodes (quantified in ≥50% of cohort) are indicated with brighter colors. ccRCC, clear cell Renal Cell Carcinoma.

Conflict of Interest—The authors declare no competing interests.

Abbreviations—The abbreviations used are: ACN, acetonitrile; AGC, automatic gain control; CPTAC, Clinical Proteome Tumor Analysis Consortium; FA, formic acid; FDR, false discovery rate; MOAC, metal oxide affinity chromatography; NAT, normal adjacent tissue; PAK, p21-activated kinases; PD, Proteome Discoverer; TCGA-KIRC, The Cancer Genome Atlas Kidney Renal Clear Cell Carcinoma.

Received September 12, 2021, and in revised form, August 23, 2022 Published, MCPRO Papers in Press, September 21, 2022, https://doi.org/10.1016/j.mcpro.2022.100417

REFERENCES

1. Craven, R. A., Vasudev, N. S., and Banks, R. E. (2013) Proteomics and the search for biomarkers for renal cancer. *Clin. Biochem.* **46**, 456–465
2. Capitanio, U., and Montorsi, F. (2016) Renal cancer. *Lancet* **387**, 894–906
3. Cooper S, J., Tun H, W., Roper S, M., and Kim, Y. (2012) Current status of biomarker discovery in human clear cell renal cell carcinoma. *J. Mol. Biomarkers Diagn.* https://doi.org/10.4172/2155-9929.S2-005
4. Ardito, F., Giuliani, M., Perrone, D., Troiano, G., and Lo Muzio, L. (2017) The crucial role of protein phosphorylation in cell signaling and its use as targeted therapy (Review). *Int. J. Mol. Med.* **40**, 271–280
5. Humphrey, S. J., James, D. E., and Mann, M. (2015) Protein phosphorylation: a major switch mechanism for metabolic regulation. *Trends Endocrinol. Metab.* **26**, 676–687
6. Harsha, H. C., and Pandey, A. (2010) Phosphoproteomics in cancer. *Mol. Oncol.* **4**, 482–495
7. Deb, B., Sengupta, P., Sambath, J., and Kumar, P. (2020) Bioinformatics analysis of global proteomic and phosphoproteomic data sets revealed activation of NEK2 and AURKA in cancers. *Biomolecules* **10**, 237
8. Clark, D. J., Dhanasekaran, S. M., Petralia, F., Pan, J., Song, X., Hu, Y., *et al*. (2019) Integrated proteogenomic characterization of clear cell renal cell carcinoma. *Cell* **179**, 964–983.e31
9. Peng, X., Xu, F., Liu, S., Li, S., Huang, Q., Chang, L., *et al*. (2017) Identification of missing proteins in the phosphoproteome of kidney cancer. *J. Proteome Res.* **16**, 4364–4373
10. Haake, S. M., Li, J., Bai, Y., Kinose, F., Fang, B., Welsh, E. A., *et al*. (2016) Tyrosine kinase signaling in clear cell and papillary renal cell carcinoma revealed by mass spectrometry-based phosphotyrosine proteomics. *Clin. Cancer Res.* **22**, 5605–5616
11. Senturk, A., Sahin, A. T., Armutlu, A., Kiremit, M. C., Acar, O., Erdem, S., *et al*. (2021) Quantitative proteomics identifies secreted diagnostic biomarkers as well as tumor-dependent prognostic targets for clear cell renal cell carcinoma. *Mol. Cancer Res.* **19**, 1322–1337
12. Zhou, H., Ye, M., Dong, J., Corradini, E., Cristobal, A., Heck, A. J., *et al*. (2013) Robust phosphoproteome enrichment using monodisperse microsphere-based immobilized titanium (IV) ion affinity chromatography. *Nat. Protoc.* **8**, 461–480
13. Kall, L., Canterbury, J. D., Weston, J., Noble, W. S., and MacCoss, M. J. (2007) Semi-supervised learning for peptide identification from shotgun proteomics datasets. *Nat. Met.* **4**, 923–925
14. Mi, H., Muruganujan, A., Ebert, D., Huang, X., and Thomas, P. D. (2019) PANTHER version 14: more genomes, a new PANTHER GO-slim and improvements in enrichment analysis tools. *Nucl. Acids Res.* **47**, D419–D426
15. Sondka, Z., Bamford, S., Cole, C. G., Ward, S. A., Dunham, I., and Forbes, S. A. (2018) The COSMIC cancer gene census: describing genetic dysfunction across all human cancers. *Nat. Rev. Cancer* **18**, 696–705
16. Wishart, D. S., Feunang, Y. D., Guo, A. C., Lo, E. J., Marcu, A., Grant, J. R., *et al*. (2018) DrugBank 5.0: a major update to the DrugBank database for 2018. *Nucl. Acids Res.* **46**, D1074–D1082
17. Uretmen Kagiali, Z. C., Sanal, E., Karayel, O., Polat, A. N., Saatci, O., Ersan, P. G., *et al*. (2019) Systems-level analysis reveals multiple modulators of epithelial-mesenchymal transition and identifies DNAJB4 and CD81 as novel metastasis inducers in breast cancer. *Mol. Cell Proteomics* **18**, 1756–1771
18. Ochoa, D., Jarnuczak, A. F., Vieitez, C., Gehre, M., Soucheray, M., Mateus, A., *et al*. (2020) The functional landscape of the human phosphoproteome. *Nat. Biotechnol.* **38**, 365–373
19. Horn, H., Schoof, E. M., Kim, J., Robin, X., Miller, M. L., Diella, F., *et al*. (2014) KinomeXplorer: an integrated platform for kinome biology studies. *Nat. Met.* **11**, 603–604
20. Binns, D., Dimmer, E., Huntley, R., Barrell, D., O'Donovan, C., and Apweiler, R. (2009) QuickGO: a web-based tool for gene ontology searching. *Bioinformatics* **25**, 3045–3046
21. Liao, Y., Wang, J., Jaehnig, E. J., Shi, Z., and Zhang, B. (2019) WebGestalt 2019: gene set analysis toolkit with revamped UIs and APIs. *Nucl. Acids Res.* **47**, W199–W205
22. Eid, S., Turk, S., Volkamer, A., Rippmann, F., and Fulle, S. (2017) KinMap: a web-based tool for interactive navigation through human kinome data. *BMC Bioinform.* **18**, 16
23. Cheng, A., Grant, C. E., Noble, W. S., and Bailey, T. L. (2019) MoMo: discovery of statistically significant post-translational modification motifs. *Bioinformatics* **35**, 2774–2782
24. Gyorffy, B., Lanczky, A., Eklund, A. C., Denkert, C., Budczies, J., Li, Q., *et al*. (2010) An online survival analysis tool to rapidly assess the effect of 22, 277 genes on breast cancer prognosis using microarray data of 1,809 patients. *Breast Cancer Res. Treat* **123**, 725–731
25. Cancer Genome Atlas Research, N. (2013) Comprehensive molecular characterization of clear cell renal cell carcinoma. *Nature* **499**, 43–49
26. Hornbeck, P. V., Zhang, B., Murray, B., Kornhauser, J. M., Latham, V., and Skrzypek, E. (2015) PhosphoSitePlus, 2014: mutations, PTMs and recalibrations. *Nucl. Acids Res.* **43**, D512–D520
27. Sharma, P., Alsharif, S., Fallatah, A., and Chung, B. M. (2019) Intermediate filaments as effectors of cancer development and metastasis: a focus on keratins, vimentin, and nestin. *Cells* **8**, 497
28. Kamacioglu, A., Tuncbag, N., and Ozlu, N. (2021) Structural analysis of mammalian protein phosphorylation at a proteome level. *Structure* **29**, 1219–1229.e3
29. Rust, H. L., and Thompson, P. R. (2011) Kinase consensus sequences: a breeding ground for crosstalk. *ACS Chem. Biol.* **6**, 881–892
30. Brenner, W., Färber, G., Herget, T., Wiesner, C., Hengstler, J. G., and Thüroff, J. W. (2003) Protein kinase C eta is associated with progression of renal cell carcinoma (RCC). *Anticancer Res.* **23**, 4001–4006
31. An, J., Liu, H., Magyar, C. E., Guo, Y., Veena, M. S., Srivatsan, E. S., *et al*. (2013) Hyperactivated JNK is a therapeutic target in pVHL-deficient renal cell carcinoma. *Cancer Res.* **73**, 1374–1385
32. Osborne, C. K. (1998) Tamoxifen in the treatment of breast cancer. *New Engl. J. Med.* **339**, 1609–1618
33. Ye, D. Z., and Field, J. (2012) PAK signaling in cancer. *Cell Logist.* **2**, 105–116
34. Liu, H., Liu, K., and Dong, Z. (2021) The role of p21-activated kinases in cancer and beyond: where are we heading? *Front. Cell Dev. Biol.* **9**, 641381
35. Rini, B. I., Campbell, S. C., and Escudier, B. (2009) Renal cell carcinoma. *Lancet* **373**, 1119–1132
36. Xue, Y., Bi, F., Zhang, X., Zhang, S., Pan, Y., Liu, N., *et al*. (2006) Role of Rac1 and Cdc42 in hypoxia induced p53 and von Hippel-Lindau suppression and HIF1alpha activation. *Int. J. Cancer* **118**, 2965–2972
37. Druker, J., Wilson, J. W., Child, F., Shakir, D., Fasanya, T., and Rocha, S. (2021) Role of hypoxia in the control of the cell cycle. *Int. J. Mol. Sci.* **22**, 4874
38. Sawant, M. S., and Leube, R. E. (2017) Consequences of keratin phosphorylation for cytoskeletal organization and epithelial functions. *Int. Rev. Cell Mol. Biol.* **330**, 171–225
39. Karantza, V. (2011) Keratins in health and cancer: more than mere epithelial cell markers. *Oncogene* **30**, 127–138
40. Chowdhury, N., and Drake, C. G. (2020) Kidney cancer: an overview of current therapeutic approaches. *Urol. Clin. North Am.* **47**, 419–431
41. Perez-Riverol, Y., Csordas, A., Bai, J., Bernal-Llinares, M., Hewapathirana, S., Kundu, D. J., *et al*. (2019) The PRIDE database and related tools and resources in 2019: improving support for quantification data. *Nucl. Acids Res.* **47**, D442–D450